Journal of Ship Research, Vol. 59, No. 4, December 2015, pp. 238–245
http://dx.doi.org/10.5957/JOSR.59.4.150049

LES Applied to Ship Research

Krishnan Mahesh, Praveen Kumar, Aswin Gnanaskandan, and **Zane Nitzkorski**

Department of Aerospace Engineering and Mechanics, University of Minnesota, Minneapolis, Minnesota

Numerical simulations using the Reynolds Averaged Navier–Stokes (RANS) methodology have been widely used to study fluid problems in a variety of fields including ship research. Although computationally cheap, RANS fails to predict the fluid behavior accurately in complex flow problems where the underlying physics is dominated by unsteady complex physical phenomena. This paper discusses the use of large eddy simulation (LES) to study such complex flow physics. The predictive capability of LES is demonstrated in three complex flow problems: crashback, cavitation, and hydro-acoustics, which are of particular interest to the ship community. LES results are shown to be in good agreement with experiments for the mean and root mean square values of flow quantities in all these cases.

Keywords: hydrodynamics (propulsors); cavitation; hydroacoustics; computers in design

1. Introduction

The use of computational fluid dynamics (CFD) for the development of engineering devices is becoming more popular in recent years with the advent of powerful supercomputers. Fluid flows are being simulated using various methodologies depending on the nature of the flow problem and the availability of computational resources. These methodologies can be broadly categorized into potential methods, direct numerical simulation (DNS), Reynolds Averaged Navier–Stokes (RANS), and large eddy simulation (LES). Potential methods offer the quickest turnaround, yield accurate surface pressure for attached flows, and are invaluable for initial design. In DNS, all relevant scales of motion are resolved accurately in space and time, and no model is used. However, the computational cost associated with DNS has limited its use to study turbulent flows in simple geometries (Moin & Mahesh, 1998). The numerical simulations of fluid problems for engineering applications are most commonly performed using RANS methods. In general, RANS models work well for steady, attached flows but fail for the flow problems where the underlying physics is dominated by large-scale unsteady phenomena. LES is an intermediate method between DNS and RANS in which the large scales of motion are resolved, whereas the effect of small scales is modeled. LES is an attractive approach to predict complex turbulent flows because of its better accuracy over RANS and cheaper computational cost than DNS.

Marine flows have very high Reynolds numbers (Re) and therefore a broad range of length and time scales. The properties of the numerical algorithm used to solve the LES equations are therefore important; specifically, it is desirable that numerical dissipation not damp the smallest resolved scales and overwhelm the interscale transfer represented by the subgrid model. Mahesh et al. (2004) developed a numerical algorithm for LES of complex flows, which emphasizes discrete conservation of the kinetic energy, thus ensuring robustness at high Re without any numerical dissipation. This algorithm will be used to perform the LES reported in this paper.

In this paper, we describe the work performed at the University of Minnesota, which demonstrates the predictive capabilities of LES in three complex flow problems: crashback, hydro-acoustics, and cavitation. This paper is organized as follows. We discuss the use of LES to simulate flow over submerged bodies in crashback in Section 2. Section 3 considers the simulation of cavitation in complex flows followed by Section 4, which describes LES used to study hydro-acoustics. A brief summary in Section 5 concludes the paper.

2. Crashback

Crashback is an off-design condition in which the marine vessel moves in the forward direction whereas the propeller rotates in

Manuscript received at SNAME headquarters October 9, 2015; revised manuscript received October 12, 2015.

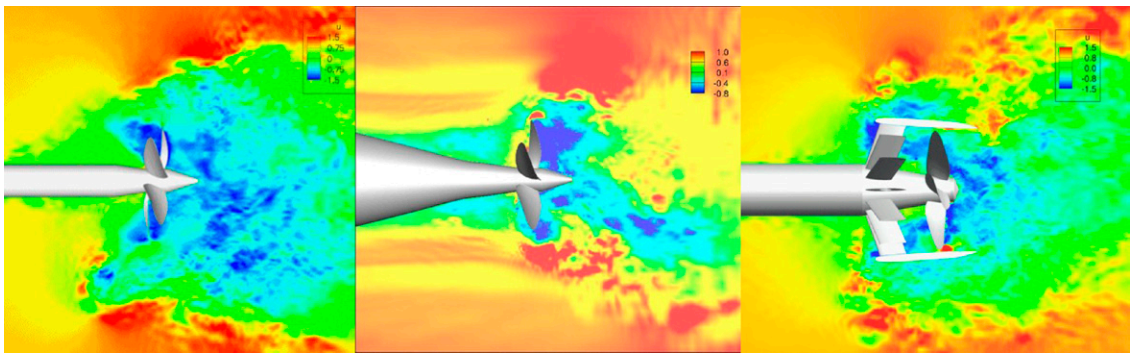

Fig. 1 Contour of instantaneous axial velocity for open propeller (left), hull-attached propeller (center) and ducted propeller with stator (right).

the reverse direction, yielding negative thrust. Flow around the propeller in crashback is characterized by large-scale unsteadiness and flow separation. High amplitude off-axis forces and moments are produced by this unsteadiness, which are transmitted to the body, adversely affecting its maneuverability. The unsteady forces can also cause damage and reduction in performance of the propeller blades. Hence, understanding crashback is critical for marine vessels.

Chen and Stern (1999) showed that RANS yield good results for the forward ($V > 0$, $n > 0$) and backward ($V < 0$, $n < 0$) modes of propeller operation where the flow is attached, but fails to accurately predict flow in crashback ($V > 0$, $n < 0$) and crashahead ($V < 0$, $n > 0$) where the flow is massively separated.

There are two major challenges associated with performing LES of hull-attached propeller in crashback: the turbulent attached flow on the body and the highly unsteady separated flow close to the propeller. The turbulent-attached boundary layer on the hull is challenging because of the small turbulent near-wall motions that determine drag. The reverse flow due to propeller rotation causes massive separation on the blades; also the flow through the propeller disc interacts with the hull wake leading to formation of a ring vortex. This unsteady separated flow is challenging because of the complicated geometry of the propeller and the low frequencies due to flow separation. Thus LES of hull-attached propeller in crashback is demanding in terms of grid generation for the complex propeller geometry and the need to run for long periods.

Our road map for flow over propelled bodies in crashback is shown in Fig. 1. We have used LES to simulate a stand-alone propeller (Jang & Mahesh 2013), hull-attached propeller (a portion of stern only) (Verma et al. 2012), and ducted propeller with stator blades (Jang & Mahesh 2008) in crashback and explained the underlying flow physics. All these simulations showed good agreement with the experimental data available in the literature (Fig. 2). We describe our ongoing work toward simulating an entire hull in crashback in this paper.

To simulate the flow over the hull, we first need to ensure that the boundary layer on the hull is captured accurately. Huang et al. (1992) and Jimenez et al. (2010) performed experiments for flow over DARPA suboff (DTMB model 5470 [Groves et al. 1989]) without appendages. Huang et al. (1992) measured pressure and skin friction coefficient on the hull along with profiles on the stern at Re = 12 million based on length. Jimenez et al. (2010) studied the intermediate wake of barehull at a Re ranging from Re = 1.1 million upto 67 million. They measured mean velocity, Reynolds stress, and turbulent intensity profiles at 3, 6, 9, 12, and 15 diameters downstream of hull and analyzed the intermediate wake of the hull. They also reported the pressure coefficient on

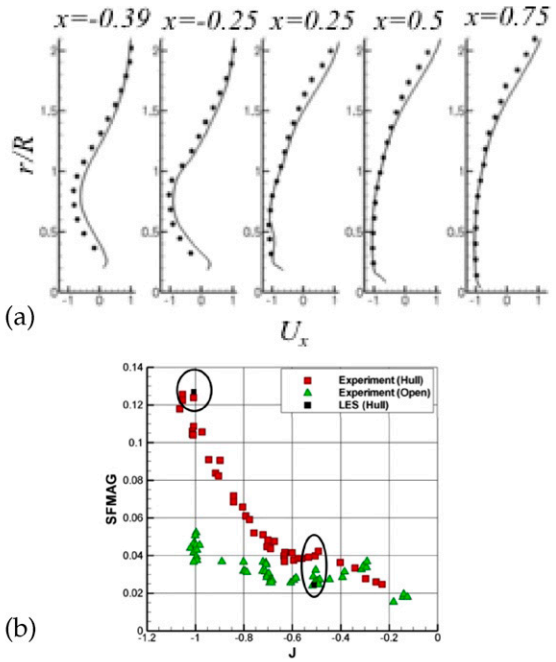

	<K_T>	σ(K_T)	<K_Q>	σ(K_Q)	<K_S>
Blade (LES)	-0.40	0.048	-0.078	9.3e-3	0.023
Blade (WT)	-0.38		-0.078		0.024
Duct (LES)	-0.069	7.1e-3	3.7e-4	4.9e-5	0.071
Stator (LES)	6.0e-3	2.4e-3	0.050	4.9e-3	0.016
Duct & Stator (LES)	-0.063	6.0e-3	0.050	4.8e-3	0.087
Duct & Stator(WT)					0.098

(c)

Fig. 2 (a) Circumferentially averaged axial velocity profiles for open propeller, x = 0 is propeller location, (b) LES reproducing the experimentally observed behavior for hull-attached propeller, and (c) LES results for loads compared to experiments for ducted propeller with stator.

the hull and computed the drag coefficient from the wake profile at different values of Re.

2.1. Simulation details

Simulations are performed in a frame of reference that rotates with the propeller. The spatially filtered incompressible Navier–Stokes equations in the rotating frame of reference are formulated for the absolute velocity vector in the inertial frame as follows:

$$\frac{\partial \overline{u}_i}{\partial t} + \frac{\partial}{\partial x_j}\left(\overline{u}_i\overline{u}_j - \overline{u}_i\varepsilon_{jkl}\omega_k x_l\right) = -\frac{\partial \overline{p}}{\partial x_i} - \varepsilon_{ijk}\omega_j\overline{u}_k + \nu\frac{\partial^2 \overline{u}_i}{\partial x_j \partial x_j} - \frac{\partial \tau_{ij}}{\partial x_j} \quad (1)$$

$$\frac{\partial \overline{u}_i}{\partial x_i} = 0$$

where, u_i is the inertial velocity in the inertial frame, p is the pressure, x_i are coordinates in the rotating noninertial reference frame, ω_j is the angular velocity of the rotating frame of reference, ν is the kinematic viscosity, ε_{ijk} denotes the permutation tensor and the approximation $\overline{u_i\varepsilon_{jkl}\omega_k x_l} \approx \overline{u}_i\varepsilon_{jkl}\omega_k x_l$ is used. The overbar $\overline{(\cdot)}$ denotes the spatial filter and $\tau_{ij} = \overline{u_i u_j} - \overline{u}_i\overline{u}_j$ is the subgrid stress. The subgrid stress is modeled by the dynamic Smagorinsky model (Germano et al. 1991; Lilly 1992). Equation (1) is solved numerically for incompressible flows on unstructured grids.

Simulations for flow over bare hull are performed using the numerical algorithm described by Mahesh et al. (2004) for LES of incompressible flow. The computational domain used for these simulations is a circular cylinder of diameter $12D$ where D is the maximum diameter of the hull. The hull is situated on the axis of this cylindrical domain such that the nose of the hull is the origin of the reference coordinate system. The domain extends $3D$ upstream of the hull and $17.2D$ downstream of the stern of the hull. Preliminary simulations (not shown here) were performd to establish that the confinement effects in the upstream and the radial directions are negligible for this domain. Freestream boundary conditions are prescribed at the inlet and the lateral boundaries and convective boundary conditions are imposed at the exit.

The computational grid contains 535 million hexahedral elements. The boundary layer hexahedral elements are extruded from the hull surface with a minimum spacing of $0.0003D$ and a growth ratio of 1.01. This corresponds to a near-wall resolution of 33, 0.5, and 11 wall units in streamwise, wall-normal and spanwise direction, respectively, at the location $x = 6$ in the hull boundary layer. The grid is partitioned into 8,192 processors and the simulations run with a time step $t = 0.0001L/U$ where L is the length of hull and U is the freestream velocity.

2.2. Results

Simulations are performed over a bare hull at a Re of 1.1 million based on hull length and the freestream velocity. The boundary layer is tripped at the same streamwise location as that of the experiments performed by Jimenez et al. (2010). This is done by imposing 5% steady wall-normal velocity perturbation at the required streamwise location. This triggers the transition of the boundary layer to turbulence with negligible addition of mass in the domain. Figure 3 show contours of instantaneous axial velocity. Both Huang et al. (1992) and Jimenez et al. (2010) report pressure coefficient on the hull but Huang et al. (1992) have corrected their pressure data for domain confinement. Huang et al. (1992) also report skin friction coefficient on the hull, whereas Jimenez et al. (2010) compute drag coefficient from the measured wake profile. Figures 4a and b shows pressure (C_p) and skin friction (C_f) coefficient on the hull, respectively, at Re = 1.1 million compared to the experiments of Huang et al. (1992), which were conducted at Re = 12 million. C_p is insensitive to Re for higher Re and C_f has been scaled based on the zero pressure gradient Re scaling ($C_f \sim \mathrm{Re}^{-0.2}$) for comparison. Our LES results show good agreement with experiments. The difference between the C_f from LES and the scaled value from Huang et al. (1992) on the stern is due to the fact that the scaling law is valid only for zero pressure gradient boundary layers. Note that the spike visible in the plot of pressure coefficient is due to tripping. Figure 4c shows the mean velocity profile at $x = 6$ on the hull. The existence of the law of the wall region and log region indicates a fully developed axial turbulent boundary layer and adequate near-wall resolution of the grid. Jimenez et al. (2010) computed drag coefficient from the measured wake profile ignoring the drag contribution of pressure and normal stress. The viscous drag coefficient predicted by LES

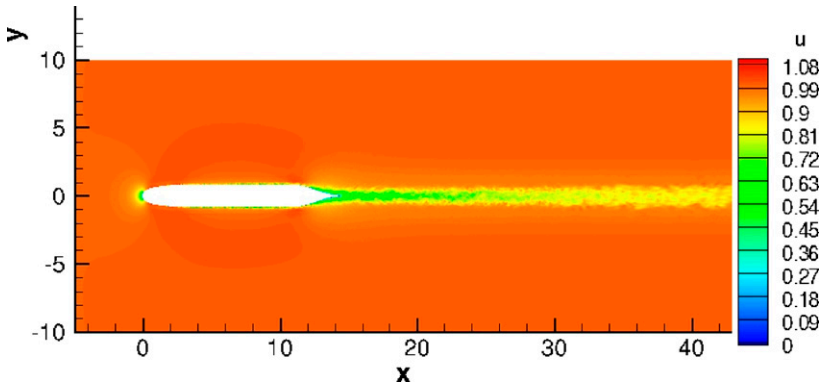

Fig. 3 Instantaneous axial velocity contours for flow over barehull at Re = 1.1 million.

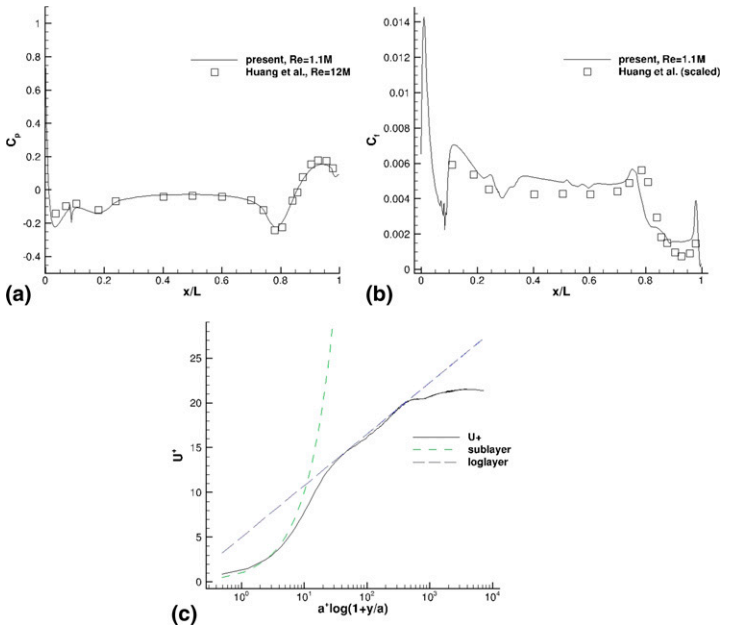

Fig. 4 (a) C_p, (b), C_f, and (c) boundary layer profile at $x = 6$ on the hull.

is 0.141, which shows good agreement with the value reported by Jimenez et al. (2010) (0.142) at Re = 1.1 million.

3. Cavitation

3.1. Physical model and numerical method

Cavitation refers to the formation of vapor when pressure in a liquid drops below vapor pressure. Sheet cavitation and its transition to cloud cavitation are of great practical interest since the highly unsteady flow can induce significant fluctuations in the thrust and torque of marine propellers. The formation of a vapor cloud is often followed by its violent collapse under high pressure, which causes material damage to the blades.

Most computational studies of sheet to cloud cavitation have employed the homogeneous mixture model (Kubota et al. 1992; Schnerr et al. 2008; Kim 2009) where the multiphase fluid mixture is treated as a single compressible fluid. Most past studies have used RANS to model the turbulence (Kunz et al. 2000; Singhal et al. 2002; Coutier-Delgosha et al. 2007; Seo & Lele 2009). However, RANS models need an ad hoc suppression of the eddy viscosity in order to predict sheet to cloud cavitation (Coutier-Delgosha et al. 2007). LES can predict flow unsteadiness without ad hoc modifications and there have been recent LES of cavitation (Bensow & Bark 2010; Dittakavi et al. 2010; Gnanaskandan & Mahesh 2015; Ji et al. 2015). A turbulent cavitating flow has a broadband spectrum, which requires non-dissipative numerical schemes to represent small scales accurately. Also, cavitation is characterized by large gradients in density, and nonlinear pressure waves formed during vapor cloud collapse. These characteristics make numerical prediction of cavitation very challenging. The numerical method of Gnanaskandan and Mahesh (2015) uses the homogeneous mixture model to represent the multiphase mixture, a characteristic based filtering to capture discontinuities, and a dynamic Smagorinsky model to represent small-scale turbulence. The governing equations are the compressible Navier–Stokes equation for the mixture of liquid and vapor along with a transport equation for vapor. The governing equations are Favre-averaged and then spatially filtered to perform LES. A dynamic Smagorinsky model is used for the subgrid terms. The unfiltered governing equations are:

$$\begin{aligned}
\frac{\partial \rho}{\partial t} &= -\frac{\partial}{\partial x_k}(\rho u_k),\\
\frac{\partial \rho u_i}{\partial t} &= -\frac{\partial}{\partial x_k}(\rho u_i u_k + p\delta_{ik} - \sigma_{ik}),\\
\frac{\partial \rho e_s}{\partial t} &= -\frac{\partial}{\partial x_k}(\rho e_s u_k - Q_k) - p\frac{\partial u_k}{\partial x_k} + \sigma_{ik}\frac{\partial u_i}{\partial x_k}\\
\frac{\partial \rho Y}{\partial t} &= -\frac{\partial}{\partial x_k}(\rho Y u_k) + S_e - S_c,
\end{aligned} \tag{2}$$

where ρ, u_i, e_s, and p are density, velocity, internal energy, and pressure, respectively, of the mixture and Y is the vapor mass fraction. The mixture density

$$\rho = \rho_l(1-\alpha) + \rho_g\alpha, \tag{3}$$

where ρ_l is the density of liquid and ρ_g is the density of vapor. α is the vapor volume fraction, which is related to the vapor mass fraction

$$\rho_l(1-\alpha) = \rho(1-Y) \quad \text{and} \quad \rho_g\alpha = \rho Y \tag{4}$$

The system is closed using a mixture equation of state (Gnanaskandan & Mahesh 2015; Seo & Lele 2009):

$$p = Y_\rho R_g T + (1-Y)\rho K_1 T\frac{p}{p+P_c} \tag{5}$$

Here, $R_g = 461.6$ J/KgK, $K_l = 2684.075$ J/KgK, and $P_c = 786.333 \times 10^6$ Pa are constants associated with the equation of state of vapor and liquid. This methodology is applied to study sheet to cloud cavitation over a wedge (Gnanaskandan & Mahesh 2014). The

simulation conditions correspond to the experiments conducted at University of Michigan (Ganesh 2015).

3.2. Transition of sheet to cloud cavitation over a wedge

The Re of the simulation based on the wedge height (h) and freestream velocity is 200,000 and the freestream cavitation number (σ) is 2.1. The computational domain is extended in both upstream ($25h$) and downstream directions ($50h$) to minimize the effect of acoustic reflection from the boundaries. Furthermore, sponge boundary conditions are used to absorb outgoing waves. Velocity and pressure are prescribed at the inlet and downstream pressure is prescribed at the outlet. No slip boundary conditions are imposed on top and bottom walls. Periodic boundary conditions are enforced at the spanwise boundaries. The computational mesh is made very fine near the wedge apex and along the entire length of the wedge where the major portion of the vapor is expected to form. The minimum grid spacing near the wedge is $0.001h \times 0.001h \times 0.01h$ in the wall normal, streamwise, and spanwise directions, respectively. The wall normal spacing stretches to $0.005h$ at a height of $0.5h$ from the wedge apex and further to about $0.01h$ at a height of h from the apex. In the streamwise direction, the grid is stretched to $0.02h$ at a distance $3.5h$ from the apex and further to $0.01h$ at the end of the wedge. The total number of control volumes is approximately 45 million. The non–dimensional time step used in the simulation is $tu_\infty/h = 1 \times 10^{-5}$.

The nature of the instantaneous solution is illustrated using isocontours of void fraction in Fig. 5, which shows the presence of both sheet and cloud cavities. The flow accelerates in the converging portion and the instantaneous pressure drops below vapor pressure at the wedge apex, which results in cavitation. The cavity then grows along the flow direction and on reaching a critical length, breaks into a cloud. This cloud is highly three dimensional and it is the collapse of this cloud that causes noise, vibration, and surface erosion. The vertical plane in Fig. 5 shows pressure contours. It can be observed that pressure exhibits both wave-like behavior (close to leading edge of the cavity) and a highly intermittent behavior (downstream of the cloud). The turbulent nature of the flow downstream prevents a coherent wave-like behavior there, since turbulence breaks up the wave thus causing highly intermittent pressure fluctuations. When a vapor cavity collapses, it creates a void and surrounding water rushes into the void creating a water hammer effect. This causes a large amount of pressure to be concentrated locally resulting in compression waves that travel in all directions. Due to confinement, these pressure waves get reflected multiple times producing a complex pressure wave pattern. These pressure waves also travel toward the inflow and modify the oncoming flow significantly.

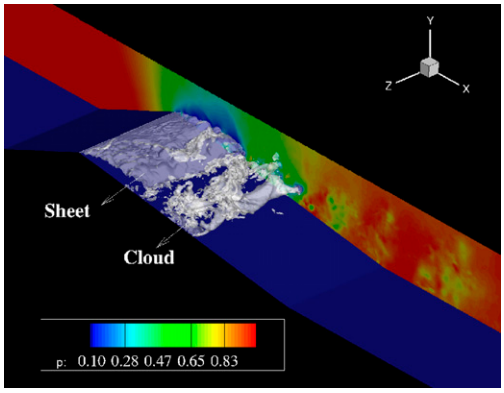

Fig. 5 Isocontours of void fraction showing sheet and cloud cavities. Side plane shows pressure contours.

The mean void fraction ($\overline{\alpha}$) at different streamwise locations on the wedge is compared to the experimental results in Fig. 6. The agreement for the mean void fraction is very good at $x/h = 0.5$ and $x/h = 3.0$ stations, (h is the height of the wedge) while LES slightly over predicts void fraction at the other two stations. Overall, the comparisons for void fraction data are encouraging suggesting the suitability of LES in predicting this highly unsteady phenomenon. The Strouhal number based on the maximum cavity length corresponding to shedding frequency obtained from the numerical simulation is $St = 0.28$, which is computed from the time histories of pressure and void fraction at several locations inside and downstream of the mean cavity. This value lies within the range of 0.25–0.3 obtained by the experiment.

4. Hydro-acoustics

Acoustic calculations using LES are a powerful predictive and reliable analysis tool for investigating the sound field produced by marine vehicles. Application to these problems requires a few key capabilities. These include the need to accurately calculate the near-field hydrodynamic fluctuations in pressure and velocity, as these are principle sound sources, a task for which LES is well suited. Another key ability required is a generalization of the boundary condition at the marine vehicle for the acoustic solver. Finally, the ability to propagate the noise to engineering distances requires an approach, which handles propagation analytically. For all these reasons, we developed a porous Ffowcs-Williams and Hawkings (1969) acoustic analogy with a novel surface extraction and endcap closure scheme Nitzkorski and Mahesh (2014).

$$p'(x,t) = \frac{x_i x_j}{4\pi c_0^2 |x|^3}\frac{\partial^2}{\partial t^2}\int_{V_{\text{ext}}}[T_{ij}]\,\mathrm{d}^3\mathrm{y} + \frac{x_i}{4\pi c_0 |x|^2}\frac{\partial}{\partial t}\int_S [\rho u_i(u_n - \upsilon_n) + P_{ij}n_j]\,\mathrm{dS} + \frac{1}{4\pi|x|}\frac{\partial}{\partial t}\int_S [\rho_0 \upsilon_n + P(u_n - \upsilon_n)]\,\mathrm{dS}. \quad (6)$$

where x_i are the location of the microphone points, T_{ij} is the Lighthill stress tensor, P_{ij} is the compressive and viscous stress tensor, and u_n and υ_n are defined at the porous surface to be the relative velocity of the fluid and the surface, respectively.

Acoustic calculations using LES and RANS have recently begun to be employed for examining sound produced from a few marine configurations. Wei and Wang (2013) investigated radiated noise from a five-bladed rotor appended SUBOFF geometry using a boundary element approach for a few points along the rotor using unsteady RANS (URANS). They also investigated vibration and modeled noise produced from structural response to varying blade loads. In Merz et al. (2009) and Caresta and Kessissoglou (2009) a stiffened body model is used in conjunction with a simplified acoustic model to obtain noise response due to bending modes and due to the propeller. LES has been applied to model

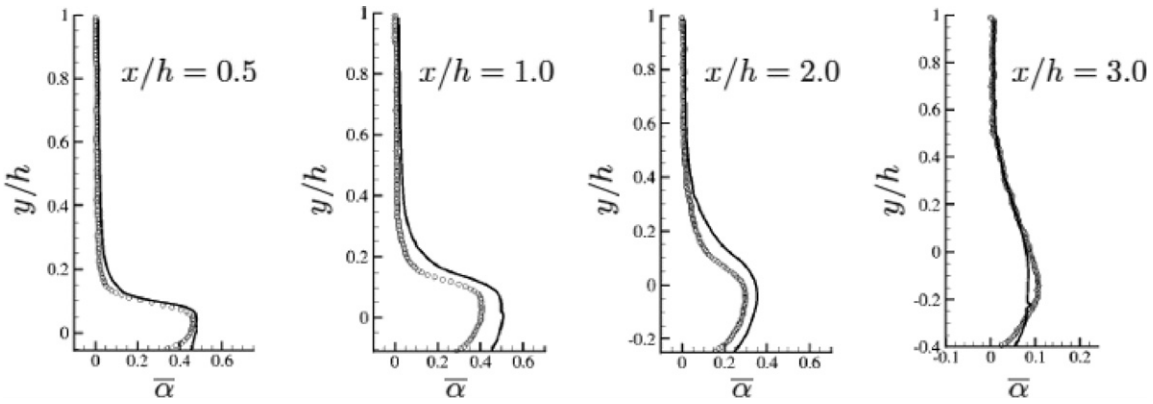

Fig. 6 Comparison of mean void fraction profiles at different streamwise locations, Symbols: Experiment, Solid: LES.

problems relevant to propellers such as airfoil noise Wang et al. (2009) and trailing edge noise Wang and Moin (2000).

4.1. Noise production from Re = 89,000 circular cylinder

In order to demonstrate the benefit of LES in wake flows, the noise from a Re = 89,000 circular cylinder is computed. This Re was chosen to compare to the experiments of Revell et al. (1977). A URANS calculation of this configuration was performed by Cox et al. (1998), which is included in our spectrum comparison. A flow and sound visualization are shown in Fig. 7a using the iso-surface of λ_2 colored by u-velocity to visualize the flow and the acoustic pressure field is projected in the background. The grid has 82 million control volumes with semicylindrical inflow of $R = 12.5D$, a rectangular outflow with $L_x = 35D$, and the span with distance πD discretized by 150 points. It has a first wall spacing of $\Delta n = 1 \times 10^{-4}$, which corresponds to a $n^+ = 0.78$. The timestep is $\Delta t = 2 \times 10^{-4}\, D/U$. The inflow is prescribed with the freestream velocity, the sides utilize a periodic boundary condition and Neumann boundary condition is prescribed at the outflow.

The recovered noise at $\theta = \pi/2$ and $r = 128D$ is compared to Revell et al. (1977) and Cox et al. (1998) in Fig. 7b and shows good agreement with experiment at the fundamental frequency as well as the drag and first lift harmonic. In contrast, the URANS predicts no harmonics of lift and drag since it is a two dimensional computation and has a larger discrepancy in the Strouhal frequency relative to current results. This sort of agreement is achievable due to the increased accuracy that LES provides for the fluctuating acoustic sources.

4.2. Noise production from 45 degree–beveled trailing edge

We have studied trailing edge noise due to its relevance to propeller noise, as most airfoil noise is dominated by trailing edge noise, and compare to the results of Olson and Mueller (2004). A flow visualization is shown in Fig. 8a illustrating the large range of scales and fluctuations associated with the velocity field which produce broadband noise. This trailing edge shape was chosen such to ensure separation leading to a large tonal component. A rescaling methodology was used to provide inflow fluctuations corresponding to turbulent boundary layers on both sides of the trailing edge, and very good agreement was obtained for the mean flow and turbulent fluctuations on the trailing edge and in its wake. The grid has 72 million points with a domain of $x/h = [-9,35]$, $y/h = [-20,20]$, and $z/h = [-\pi/2, \pi/2]$ with 150 points in the span. The tip is rounded with a radius of $r/h = 5 \times 10^{-4}$ and a

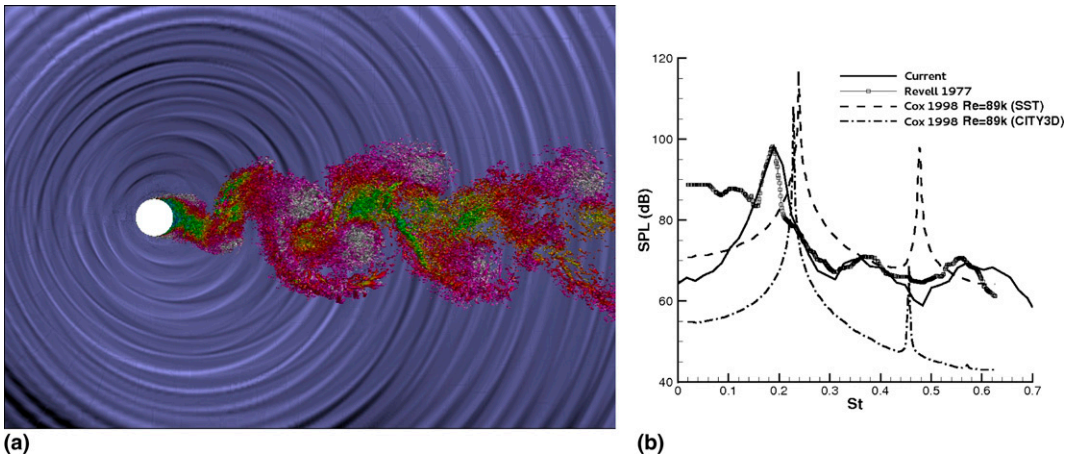

Fig. 7 (a) Flow visualization of λ_2 colored by the u-velocity with the sound field projected in the background. (b) Comparison of acoustic noise including experiment and URANS.

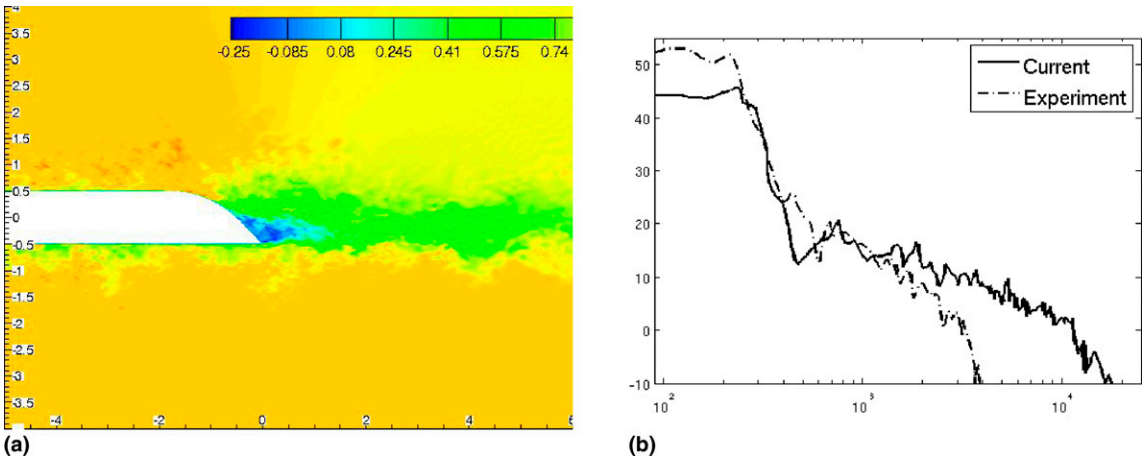

Fig. 8 (a) Flow visualization u-velocity for trailing edge configuration. (b) Comparison of sound pressure level at $x = (3, 21)$.

near-wall spacing of $\Delta n/h = 2.5 \times 10^{-5}$ near tip and $\Delta n/h = 5 \times 10^{-4}$ in the boundary layer. The timestep is $\Delta t = 1 \times 10^{-5} h/U$. Periodic boundary condition is imposed in the span and Neumann boundary condition is prescribed at the outflow.

The sound pressure level at $x = (3, 21)$ is compared between the LES and the experiment in Fig. 8b. Here, good agreement is observed. The sound pressure is smaller than experiment at lower frequencies as is common to most such comparisons between simulation and experiment. The LES predicts good agreement in broadband components. Note that the LES has higher temporal resolution than the experiment leading to increased noise predicted at higher frequencies since the experiment has a Nyquist frequency of 4,000 Hz with a 10 Hz pass-band filter.

5. Summary

LES is used to simulate three problems of considerable relevance to ship research: crashback, cavitation, and hydro-acoustics. Good agreement with experiment is demonstrated for all three problems. It is also seen that the LES predictions are better than what is obtained using RANS. LES is thus an attractive approach for predicting marine flows dominated by large-scale unsteadiness and complex physics.

Acknowledgments

This work was supported by the U.S. Office of Naval Research with Dr. Ki-Han Kim as technical monitor. Computing resources were provided by the Arctic Region Supercomputing Center of HPCMP, the Minnesota Supercomputing Institute and Argonne Leadership Computing Facility of DOE.

References

Bensow, R. E. and Bark, G. 2010 Implicit les predictions of the cavitating flow on a propeller, *Journal of Fluids Engineering*, **132**, 4, 1–10.

Caresta, M. and Kessissoglou, N. J. 2009 Structural and acoustic responses of a fluid-loaded cylindrical hull with structural discontinuities, *Applied Acoustics*, **70**, 7, 954–963.

Chen, B. and Stern, F. 1999 Computational fluid dynamics of four quadrant marine propeller flow, *Journal of Ship Research*, **43**, 4, 218–228.

Coutier-Delgosha, O., Stutz, B., Vabre, A., and Legoupil, S. 2007 Analysis of cavitating flow structure by experimental and numerical investigations, *Journal of Fluid Mechanics*, **578**, 171–222.

Cox, J. S., Brentner, K. S., and Rumsey, C. L. 1998 Computation of vortex shedding and radiated sound for a circular cylinder: subcritical to transcritical reynolds numbers, *Theoretical and Computational Fluid Dynamics*, **12**, 233–253.

Dittakavi, N., Chunekar, A., and Frankel, S. 2010 Large eddy simulation of turbulent-cavitation interactions in a venturi nozzle, *Journal of Fluids Engineering*, **132**, 12, 1–12.

Ffowcs-Williams, J. E. and Hawkings, D. L. 1969 Sound generation by turbulence and surfaces in arbitrary motion, *Philosophical Transactions of the Royal Society of London*, **264A**, 321–342.

Ganesh, H. 2015 Bubbly shock propagation as a cause of sheet to cloud transition of partial cavitation and stationary cavitation bubbles forming on a delta wing vortex. PhD thesis, University of Michigan.

Germano, M., Piomelli, U., Moin, P., and Cabot, W. H. 1991 A dynamic subgrid–scale eddy viscosity model, *Physics of Fluids. A, Fluid Dynamics*, **3**, 1760–1765.

Gnanaskandan, A. and Mahesh, K. 2014 Large eddy simulation of sheet to cloud cavitation, *Proceedings*, The 30th Symposium on Naval Hydrodynamics, November 2–7, Hobart, Australia, pp. 1–13.

Gnanaskandan, A. and Mahesh, K. 2015 A numerical method to simulate turbulent cavitating flows, *International Journal of Multiphase Flow*, **70**, 22–34.

Groves, N. C., Huang, T. T., and Chang, M. S. 1989 *Geometric Characteristics of DARPA Suboff Models:(DTRC Model Nos. 5470 and 5471)*, Annapolis, MD: David Taylor Research Center.

Huang, T., Liu, H. L., Grooves, N., Forlini, T., Blanton, J., and Gowing, S. 1992 Measurements of flows over an axisymmetric body with various appendages in a wind tunnel: the darpa suboff experimental program, *Proceedings*, The 19th Symposium on Naval Hydrodynamics, August 23–28, Seoul, Korea.

Jang, H. and Mahesh, K. 2008 Large eddy simulation of ducted propulsors in crashback, *Proceedings*, The 27th Symposium on Naval Hydrodynamics, October 5–10, Seoul, Korea.

Jang, H. and Mahesh, K. 2013 Large eddy simulation of flow around a reverse rotating propeller, *Journal of Fluid Mechanics*, **729**, 151–179.

Ji, B., Luo, X. W., Arndt, R. E. A., Peng, X., and Wu, Y. 2015 Large eddy simulation and theoretical investigations of the transient cavitating vortical flow structure around a naca66 hydrofoil, *International Journal of Multiphase Flow*, **68**, 121–134.

Jimenez, J. M., Hultmark, M., and Smits, A. J. 2010 The intermediate wake of a body of revolution at high reynolds numbers, *Journal of Fluid Mechanics*, **659**, 516–539.

Kim, S. 2009 A numerical study of unsteady cavitation on a hydrofoil, *Proceedings*, The 7th International Symposium on Cavitation, August 16–20, Ann Arbor, Michigan, pp. 1–13.

KUBOTA, A., KATO, H., AND YAMAGUCHI, H. 1992 A new modelling of cavitating flows: A numerical study of unsteady cavitation on a hydrofoil section, *Journal of Fluid Mechanics*, **240**, 1, 59–96.

KUNZ, R. F., BOGER, D. A., STINEBRING, D. R., CHYCZEWSKI, T. S., LINDAU, J. W., GIBELING, H. J., VENKATESWARAN, S., AND GOVINDAN, T. R. 2000 A preconditioned navier–stokes method for two-phase flows with application to cavitation prediction, *Computers & Fluids*, **29**, 8, 849–875.

LILLY, D. K. 1992 A proposed modification of the germano subgrid–scale closure model, *Physics of Fluids. A, Fluid Dynamics*, **4**, 3, 633.

MAHESH, K., CONSTANTINESCU, G., AND MOIN, P. 2004 A numerical method for large–eddy simulation in complex geometries, *Journal of Computational Physics*, **197**, 1, 215–240.

MERZ, S., KINNS, R., AND KESSISSOGLOU, N. 2009 Structural and acoustic responses of a submarine hull due to propeller forces, *Journal of Sound and Vibration*, **325**, 1, 266–286.

MOIN, P. AND MAHESH, K. 1998 Direct numerical simulation: a tool in turbulence research, *Annual Review of Fluid Mechanics*, **30**, 1, 539–578.

NITZKORSKI, Z. AND MAHESH, K. 2014 A dynamic end cap technique for sound computation using the ffowcs williams and hawkings equations, *Physics of Fluids*, **26**, 11, 115101.

OLSON, S. AND MUELLER, T. J. 2004 Phased array acoustic imaging of an airfoil trailing edge flow, *Proceedings*, The 11th International Symposium on Flow Visualization, August 8–12, Notre, Dame, IN.

REVELL, J. D., PRYDZ, R. A., AND HAYS, A. P. 1977 Experimental study of airframe noise vs. drag relationship for circular cylinders. Final report for nasa contract nas1-14403. Lockheed Report 28074.

SCHNERR, G. H., SEZAL, I. H., AND SCHMIDT, S. J. 2008 Numerical investigation of threedimensional cloud cavitation with special emphasis on collapse induced shock dynamics, *Physics of Fluids*, **20**, 4, 1–9.

SEO, J. H. AND LELE, S. K. 2009 Numerical investigation of cloud cavitation and cavitation noise on a hydrofoil section, *Proceedings*, The 7th International Symposium on Cavitation, August 16–20, Ann Arbor, Michigan, pp. 1–15.

SINGHAL, A. K., ATHAVALE, M. M., LI, H., AND JIANG, Y. 2002 Mathematical basis and validation of the full cavitation model, *Journal of Fluids Engineering*, **124**, 3, 617–624.

VERMA, A., JANG, H., AND MAHESH, K. 2012 The effect of an upstream hull on a propeller in reverse rotation, *Journal of Fluid Mechanics*, **704**, 61–88.

WANG, M. AND MOIN, P. 2000 Computation of trailing-edge flow and noise using large-eddy simulation, *AIAA Journal*, **38**, 12, 2201–2209.

WANG, M., MOREAU, S., IACCARINO, G., AND ROGER, M. 2009 Les prediction of wall-pressure fluctuations and noise of a low-speed airfoil, *International Journal of Aeroacoustics*, **8**, 3, 177–197.

WEI, Y. AND WANG, Y. 2013 Unsteady hydrodynamics of blade forces and acoustic responses of a model scaled submarine excited by propeller's thrust and side-forces, *Journal of Sound and Vibration*, **332**, 8, 2038–2056.